

Article

Shape-Controlled TiC_x Particles Fabricated by Combustion Synthesis in the Cu-Ti-C System

Dongdong Zhang ¹, Haolong Liu ¹, Liping Sun ², Fang Bai ¹, Yong Wang ¹ and Jinguo Wang ^{1,*}

¹ Key Laboratory of Automobile Materials of Ministry of Education, Department of Materials Science and Engineering, Jilin University, Changchun 130025, China; dong525925@163.com (D.Z.); idbicdi@163.com (H.L.); hljsunlp@163.com (L.S.); jidabaifang@163.com (F.B.); wynn1209@163.com (Y.W.)

² COSCO Logistics (Beijing) Materials Co., Ltd, No. 3 Maizidian West Road, Beijing 100016, China

* Correspondence: jgwang@jlu.edu.cn; Tel./Fax: +86-431-8509-4699

Academic Editor: Roberto Comparelli

Received: 17 May 2017; Accepted: 4 July 2017; Published: 6 July 2017

Abstract: TiC_x particle-reinforced Cu-matrix composites were prepared in the Cu-Ti-C system by thermal explosion and hot press. Extracted TiC_x particles with various shapes of in situ TiC_x particles in the Cu-Ti-C system were observed through the Field Emission Scanning Electron Microscope (FESEM). It was found that octahedral and close-to-spherical, spherical or cubic TiC_x could be fabricated by changing the C/Ti molar ratio and Cu content. Then, the effect of the C/Ti molar ratio and constituent element concentrations on the shape of in situ TiC_x particles was determined: the shape of TiC_x particles is octahedral at a C/Ti ratio of 0.4–0.6 with the presence of 70 vol% Cu; or spherical and close-to-spherical at 0.8–1.0 with the presence of 70 vol% Cu; or cubic at C/Ti ratios ≥ 1.0 with the presence of Cu from 80 vol%–90 vol% and even at C/Ti ratios >1.0 with the presence of 70 vol% Cu. The shape-controlled synthesis of TiC_x particles in the Cu-Ti-C system is realized.

Keywords: in situ TiC_x; molar ratio; shape-controlled; thermal explosion

1. Introduction

Titanium carbide (TiC_x), a typical transition metal carbide, is the most widely-used phase of particle-reinforced metal matrix composites owing to its high melting point [1,2], high Young's modulus [3,4], low density [5,6] and excellent conductive and thermal performances [7,8]. It is well known that the shape of ceramic particles is pivotal for the performance, especially mechanical performance, of ceramic particle-reinforced metal matrix composites [9–11]. For example, Meijer et al. [12] studied the effect of cube-shaped and spherically-shaped particles on the mechanical performance by Finite Element Analysis (FEA), and the results showed that sharp-cornered cubic particles contributed to enhancing the mechanical performance of the composites. However, the stress concentration near the edges and corners of cubic particles would reduce the elongation of composites.

As we known, the combustion synthesis is the optimal way to prepare TiC_x particle-reinforced metal matrix composites [13–20]. The shape of TiC_x particles in metal matrix can be controlled through the alteration of kinetics and thermodynamic conditions during combustion synthesis. As reported, with the increase in the C/Ti molar ratio in the Al-Ti-C system, the shape of TiC_x particles changed from octahedron to truncated octahedron to close-to-sphere to sphere [21]. Nie et al. [22] found that the addition of Ni into the Al-Ti-C system can effectively inhibit the growth of {100} surfaces and successfully prepared cube-shaped TiC_x particles. Wang et al. [23] fabricated 40–60 vol% TiC_x/Al composites by using C-black as the carbon source in the Al-Ti-C system. They found that the main morphologies of the reinforcing particles were sphere and close-to-sphere. As described above, research on the shape of combustion-synthesized TiC_x particles was focused on the Al matrix [24–26], but rarely on the shape-controlled synthesis of TiC_x particles in Cu-matrix composites. As is well known, TiC_x

particle-enhanced copper matrix composite is a widely-used material in engineering and the functional materials field for its outstanding properties, such as excellent electrical and thermal conductivities, good corrosion resistance and ease of fabrication [27–31]. Therefore, it is imperative to study the shape of reinforcing particles of the in situ TiC_x/Cu composite.

Carbon Nanotubes (CNT) of high chemical activity comprise a key factor of fabricating smaller TiC_x particles than other carbon sources. This kind of small C source is conducive for [C] atoms to dissolve into the Cu-Ti liquid phase to form the Cu-Ti-C ternary liquid phase, reducing the heat for the dissolution of [C] atoms compared with a large C source, which would contribute to the decrease of the TiC_x particle size. According to the viewpoint of Jin et al. [21], the addition of a second metal (Me) such as Al, Cu and Fe can also decrease the combustion temperature and thus prevent the ceramic particles from further growth. For example, with the increase in the Al incorporation from 10–40 wt%, the sizes of the TiC_x particles decrease from about 3 μm down to 400 nm. However, when more Me (≥ 50 wt%) is incorporated, the self-propagating high-temperature synthesis reaction tends to be incomplete or even cannot be ignited. Generally, this situation can be improved through using finer C-source particles because they can enlarge the area of the contact surface between the liquid and the carbon source and decrease the activation energy of the SHS reaction. According to Wang et al.'s study [32], elevated temperature creep resistance of the Al-Cu-Mg alloy is actually enhanced due to the presence of in situ nano-sized TiC_x particles using CNTs as the C source. Therefore, CNTs with high chemical activity were the preferred C source to fabricate small-sized and low-content TiC_x particle-reinforced copper matrix composites.

According to a previous study, the shape of TiC_x particles is mainly decided by the post-nucleation growth rates of different crystal planes [33,34]. When the {100} surfaces grows faster than that of the {111} surfaces, the shape of TiC_x particles is octahedral; otherwise, the shape is cubic. However, it is still unclear what the factors that influence the growth rates of crystal planes are. Despite many efforts having been performed on the shape change of combustion-synthesized ceramic particles, only limited work has been conducted on the shape evolution laws of ceramic particles and how to realize the shape-controlled synthesis of ceramic particles [22,33]. However, no study has been concerned with how to achieve particle-shape macro-control of in situ TiC_x particles, making the present investigation necessary.

In this work, Thermal Explosion (TE) and Hot Press (HP) are combined to prepare in situ TiC_x particle-reinforced Cu-matrix composites in the Cu-Ti-C system. By altering the kinetics conditions in the Cu-Ti-C system, ceramic particles with different shapes were prepared. The morphologic changes of TiC_x particles under different kinetics conditions are investigated, and the shape variation law of combustion-synthesized ceramic particles is explored, aiming to realize the shape-controlled synthesis of TiC_x particles in Cu-matrix composites. Furthermore, this will be the first time that cube-shaped TiC_x in the Cu-Ti-C system are prepared by the method of TE and HP consolidation. These results can provide an important reference value for controlling the shape of TiC_x to meet different requirements.

2. Experimental Details

The raw materials used here were from commercial powders of Cu ($\sim 48 \mu m$), titanium ($\sim 25 \mu m$) and CNTs (~ 15 – $100 \mu m$ in length and 10–30 nm in diameter). The powders were mixed in a Ti/C molar ratio of 1:1 with different Cu contents (90 vol%, 80 vol%, 70 vol%, 60 vol%, 50 vol%) and various Ti/C molar ratios (0.4, 0.6, 0.8, 1.0, 1.2 and 1.4) with Cu contents of 30 vol%. The powders were mixed sufficiently by ball milling in a ceramic wall container for 24 h and then pressed into preforms in dimensions of 28 mm in diameter and 55 mm in height at room temperature. The TE experiments were conducted in a self-made vacuum thermal explosion furnace as illustrated in Figure 1. The preforms were first put into a high strength graphite mold, and then, the graphite mold was placed in the vacuum thermal explosion furnace and heated at the heating rate of 30 $^{\circ}C/min$ under an atmosphere of high purity argon (purity $\sim 99.999\%$) to prevent the oxidation of Cu and carbon burning loss. Once the temperature, which was measured by a thermocouple, rose rapidly, the preform was immediately

pressed by a uniaxial compression of 40 MPa for 60 s. The composite was successfully fabricated when the temperature cooled down to room temperature.

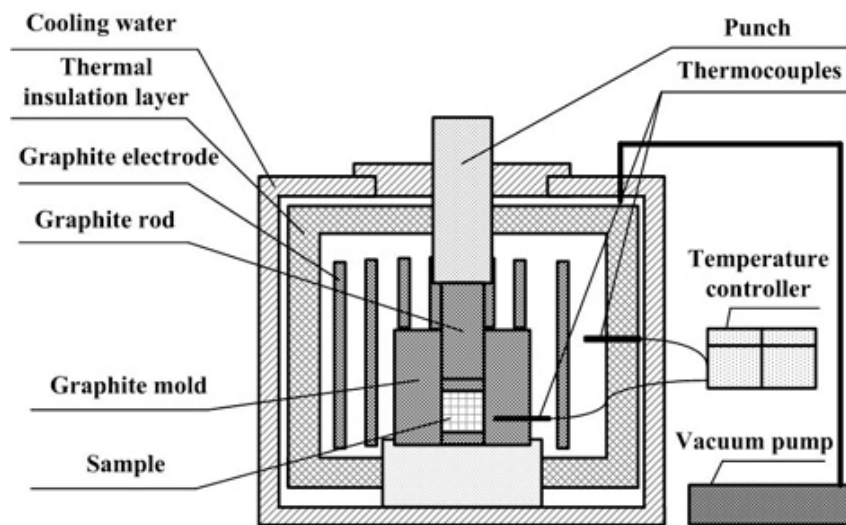


Figure 1. Schematic of the equipment for the Thermal Explosion (TE) and Hot Press (HP) consolidation experiment.

The phase components of the composites were characterized using X-ray diffraction (XRD, Rigaku D/Max 2500PC, Tokyo, Japan). The bulk samples were then dissolved in a FeCl_3 -HCl distilled water solution to remove the Cu coating on the surfaces of the TiC_x particles. The morphologies of the extracted TiC_x particles were then observed using a Field Emission Scanning Electron Microscope (FESEM, JSM 6700F, Tokyo, Japan) and High Resolution Transmission Electron Microscopy (HRTEM, JEM-2100F, Tokyo, Japan).

3. Results and Discussion

The XRD patterns of 30 vol% TiC_x /Cu composites with C/Ti molar ratios of 0.4, 0.6, 0.8, 1.0, 1.2 and 1.4 are shown in Figure 2. The diffraction peaks belonging to TiC_x and Cu corresponding to each sample can be seen clearly. Ti_3Cu was only detected when the C/Ti molar ratio was equal to or lesser than 0.6. Figure 3 shows the FESEM images of extracted TiC_x particles from TiC_x /Cu composites with C/Ti molar ratios of 0.4, 0.6, 0.8, 1.0, 1.2 and 1.4. It can be seen that the morphology of TiC_x particles shows an obvious dependence on the C/Ti molar ratio when the Cu content is defined. When the C/Ti molar ratio was below 0.6, close-to-octahedrally- and octahedrally-shaped TiC_x were observed (Figure 3a,b); when the C/Ti molar ratio was between 0.6 and 1.0, spherical and close-to-spherical TiC_x were the main shapes of the TiC_x particles in the composites; and when the C/Ti molar ratio exceeded 1.0, cube-shaped TiC_x particles were observed. Figure 4 is the TEM images of (a) octahedral, (b) spherical and (c) cubic TiC_x particles with various C/Ti molar ratios corresponding to the results of Figure 3. The cube- TiC_x particles are surrounded closely by the Cu matrix, and there is a good interface between TiC_x particles and the Cu matrix, as shown in Figure 4. The good interface bonding is beneficial to improve the strength of the composites.

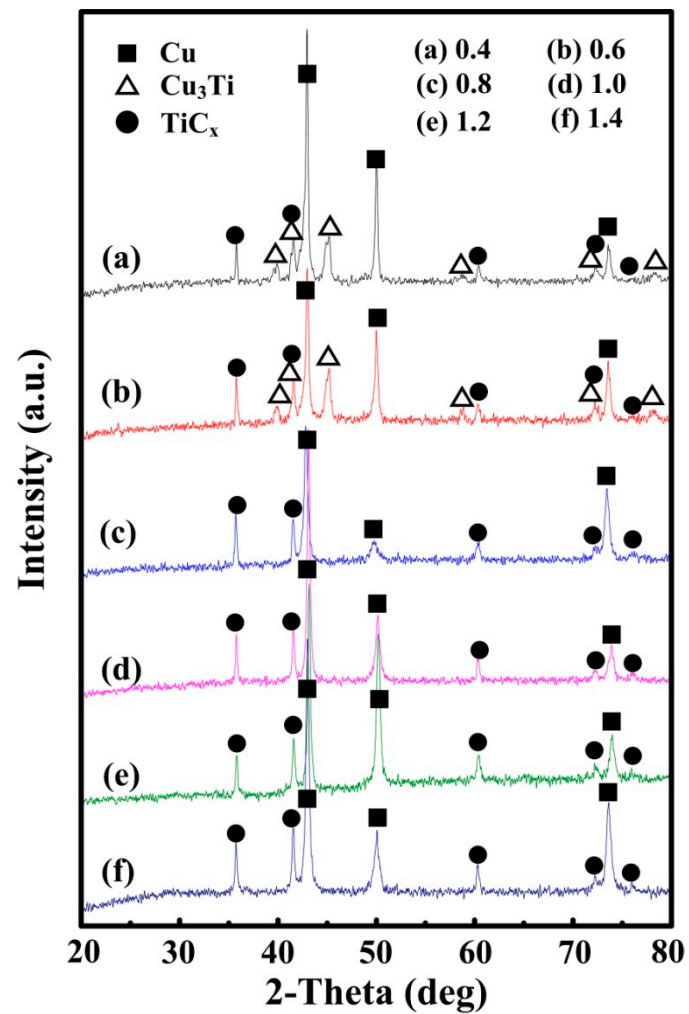


Figure 2. XRD patterns of the Thermal Explosion (TE) + Hot Press (HP) reaction products in the 70 vol% Cu-Ti-C samples with different C/Ti molar ratios: (a) 0.4, (b) 0.6, (c) 0.8, (d) 1.0, (e) 1.2 and (f) 1.4.

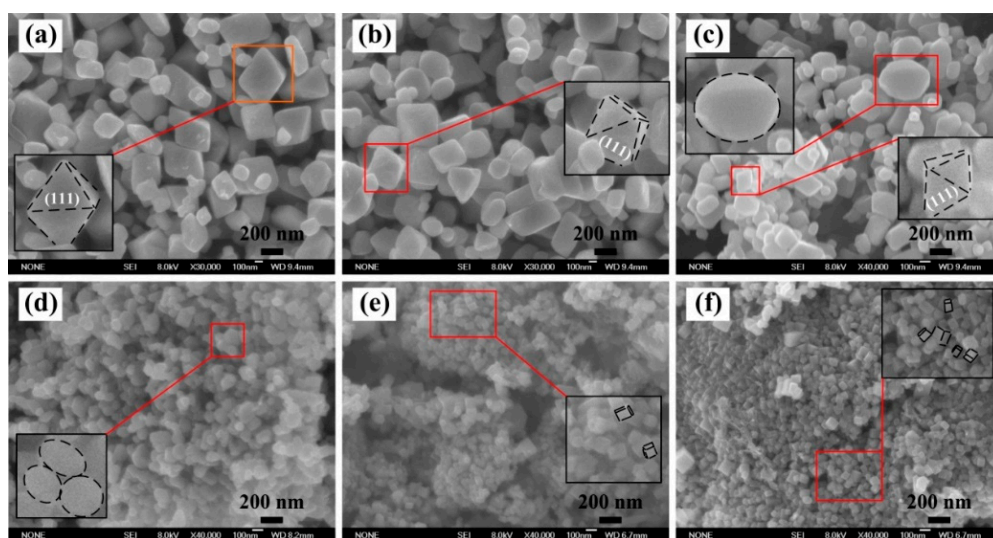


Figure 3. Morphologies of the TiC_x particles formed in the Cu-Ti-C samples with different C/Ti molar ratios: (a) 0.4 (b) 0.6 (c) 0.8 (d) 1.0 (e) 1.2 and (f) 1.4.

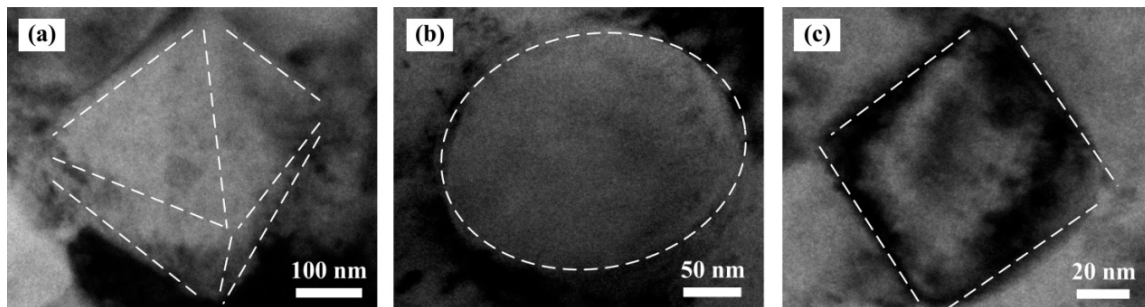


Figure 4. TEM images of (a) octahedral, (b) spherical and (c) cubic TiC_x particles with various C/Ti molar ratios.

Figure 5 shows the XRD patterns of TiC_x/Cu composites with a C/Ti molar ratio of 1.0 and Cu content of 90, 80, 70, 60 and 50 vol% in the composites. Figure 6 shows the morphologies of the TiC_x particles after extraction. It can be obviously seen from Figure 5 that the composites mainly are composed of the Cu and TiC_x phases. No other intermediate phases are detected in these samples. When the C/Ti molar ratio is constant, the shape of TiC_x particles gradually changes from cube to close-to-spherical to spherical with the decrease in Cu content. Thus, we can conjecture that the shapes of in situ TiC_x particles may be affected by not only the C/Ti molar ratio, but also the content of constituent elements in the Cu-Ti-C system.

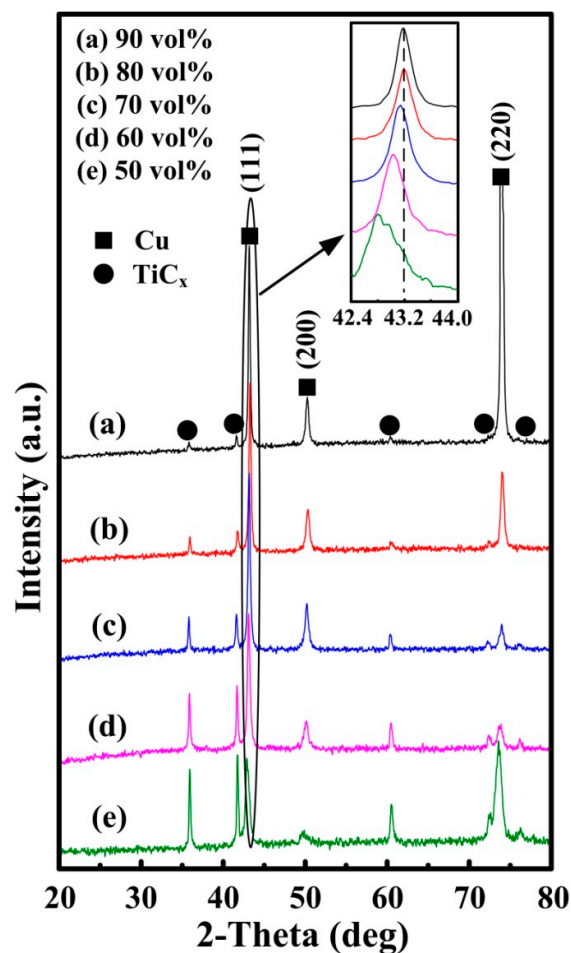


Figure 5. XRD patterns of the TE + HP reaction products in Cu-Ti-C samples with different Cu contents: (a) 90 vol%, (b) 80 vol%, (c) 70 vol%, (d) 60 vol% and (e) 50 vol%.

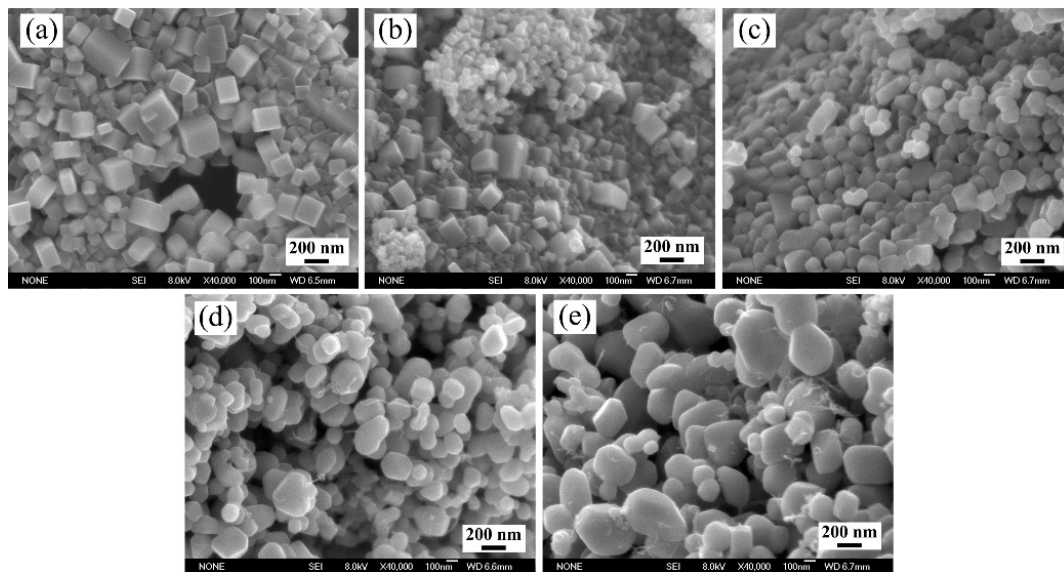


Figure 6. Morphologies of the TiC_x particles in the Cu-Ti-C system with different Cu contents: (a) 90 vol%, (b) 80 vol%, (c) 70 vol%, (d) 60 vol% and (e) 50 vol%.

The XRD patterns of TiC_x/Cu composites shown in Figures 2 and 5 showed that TiC_x particles could be successfully synthesized by TE and HP in the Cu-Ti-C system. Moreover, in addition to the main phase constitutions, i.e., Cu and TiC_x phases, the Cu_3Ti phase was also detected in these samples when the C/Ti molar ratio was equal to or less than 0.6 (Figure 2), indicating that not all of the Ti was involved in the in situ reaction. However, Ti and C phases were not detected in the composites when the C/Ti molar ratio was higher than 0.6. In addition, the (111) diffraction peaks of the composites with the Cu content of 70, 60 and 50 vol% (Figure 5) shifted to lower angles compared with those of the composites with the Cu contents of 90 and 80 vol%. This indicated that some Ti atoms entered into the crystal lattice of Cu and then formed the Cu solid solution [35]. Accordingly, it can be confirmed that Ti was residual for the Cu content of 70, 60 and 50 vol% in TiC_x/Cu composites.

As already discussed, the eventual shape of in situ TiC_x has a direct correlation with the x value. The actual x value can be calculated by combining XRD results with the curve fitting the lattice constant and the C/Ti molar ratio [36]. The calculated x value of the cube-shaped TiC_x with 90 vol% Cu content at a C/Ti molar ratio of 1.0 was 0.92. The calculated x value of octahedrally-shaped one with 70 vol% Cu content at a C/Ti molar ratio of 0.4 was 0.62, respectively. Accordingly, the structure of TiC_x for cube-shaped TiC_x with an x value of about 1.0 and octahedrally-shaped TiC_x with an x value about 0.625 was established to explain how the concentration affects the shape of in situ TiC_x according to the 64-atom supercell with different stoichiometries [33]. As shown in Figure 7, the C atom vacancies appeared with the decrease of the x value. Degtyareva et al. [37] held that vacancy is a key factor for the stability of the *fcc* structure. The amount of C atoms in the C atom vacancy structure was less than the structure without vacancy. As a result, low [C] contributed to the atom vacancy in the formation of the TiC_x crystal. When [C] is very low, the Cu-Ti-C ternary liquid cannot provide enough C atoms. Thus, it cannot grow into cubes, but instead, into spheres. With the decrease of [C], more vacancies formed, and this would grow into octahedrons. On the contrary, with the increase of [C], the Cu-Ti-C ternary liquid can provide enough C atoms to form cube-shaped TiC_x .

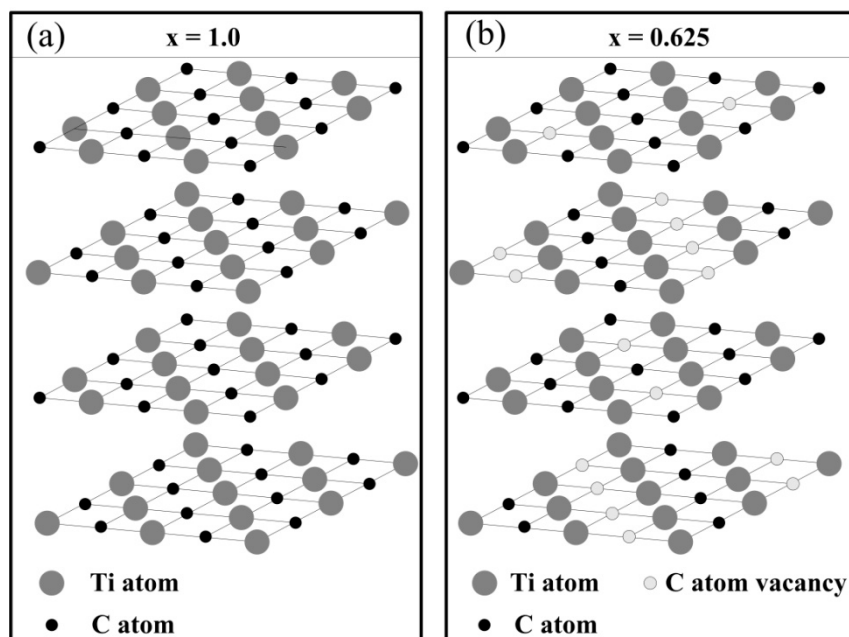


Figure 7. Atomic structures of TiC_x (a) $x = 1$ and (b) $x = 0.625$.

We now turn to the TiC_x/Cu composites with a C/Ti molar ratio of 1.0 and Cu content of 90, 80, 70, 60 and 50 vol%. For the Cu content of 90 vol% TiC_x/Cu composite, the TiC_x particles are cubic shaped, which is consistent with the calculations based on first principle [34,38]. However, when the Cu content gradually decreases, the shape of TiC_x particles changed from cube, close-to-sphere, to sphere gradually. Models of the reaction mechanism with different Cu contents were built to explain the unequable results, as shown in Figure 8.

The ceramic-phase combustion synthesis is a high-temperature, rapid, nonlinear and nonstationary transfer process (energy, mass and momentum), accompanied by many complex chemical and physical phenomena. Thus, the influence factors on the growth of ceramic particles are very complex [39]. As is known, the in situ reaction of high metal content is that of self-propagating high-temperature synthesis, and low metal content is that of thermal explosion. According to the reaction mechanism in the Cu-Ti-C system [40,41], the in situ synthesis of TiC_x necessitates the mutual diffusion and encounter of Ti and C atoms. However, C atoms are hardly soluble in Cu, which modestly limits the transmission speed and distance of C atoms. As for the models of the reaction mechanism with different Cu contents shown in Figure 8, Ti_xCu_y was firstly formed with the increase of the temperature, as shown in Figure 8b,g; the Cu-Ti liquid formed when it reached the melting point of Ti_xCu_y , and the Cu-Ti liquid spread over the CNTs (Figure 8c,h), leading the atoms in CNT to dissolve into the Cu-Ti liquid to form the Cu-Ti-C ternary liquid. Subsequently, a number of TiC_x firstly formed close to the CNTs, as shown in Figure 8d,i. When the Cu content is high, the C atoms' transmission speed is sluggish, and the transmission distance between C and Ti atoms is very far. Accordingly, the slow reaction speed left enough time for C atoms to dissolve from CNTs into the liquid, as well as the encountering and reaction of C atoms and Ti atoms. The concentration of C atoms is high and that of Ti atoms low near the CNTs, as shown in Figure 8d. Thus, the concentration gradient and the local atom shortage of Ti occurred in some spaces near the CNTs, which led to the abundance of reacting C atoms, making the C/Ti atom ratio close to one, thereby forming the cube-shaped TiC_x particles, as shown in Figure 8e. The exothermic combustion synthesis led to the continuing rise of temperature in the reaction system [42], so the residual CNTs and Ti successively reacted. When the Cu content is low, the distance between Ti and CNTs was very short, so the transmission distance between Ti and C atoms was shortened. Upon the reaction between Ti and C atoms, more Ti atoms would transmit to the vicinity of CNTs within a short time, such that C atoms were unable to dissolve

from CNTs for the fast reaction speed, resulting in the C/Ti atom ratio being smaller than one, and finally, close-to-spherical TiC_x particles were formed, as shown in Figure 8j. As a result, the shape of TiC_x particles with 90 and 80 vol% Cu content was cubic and with 70, 60 and 50 vol% Cu content was spherical and close-to-spherical.

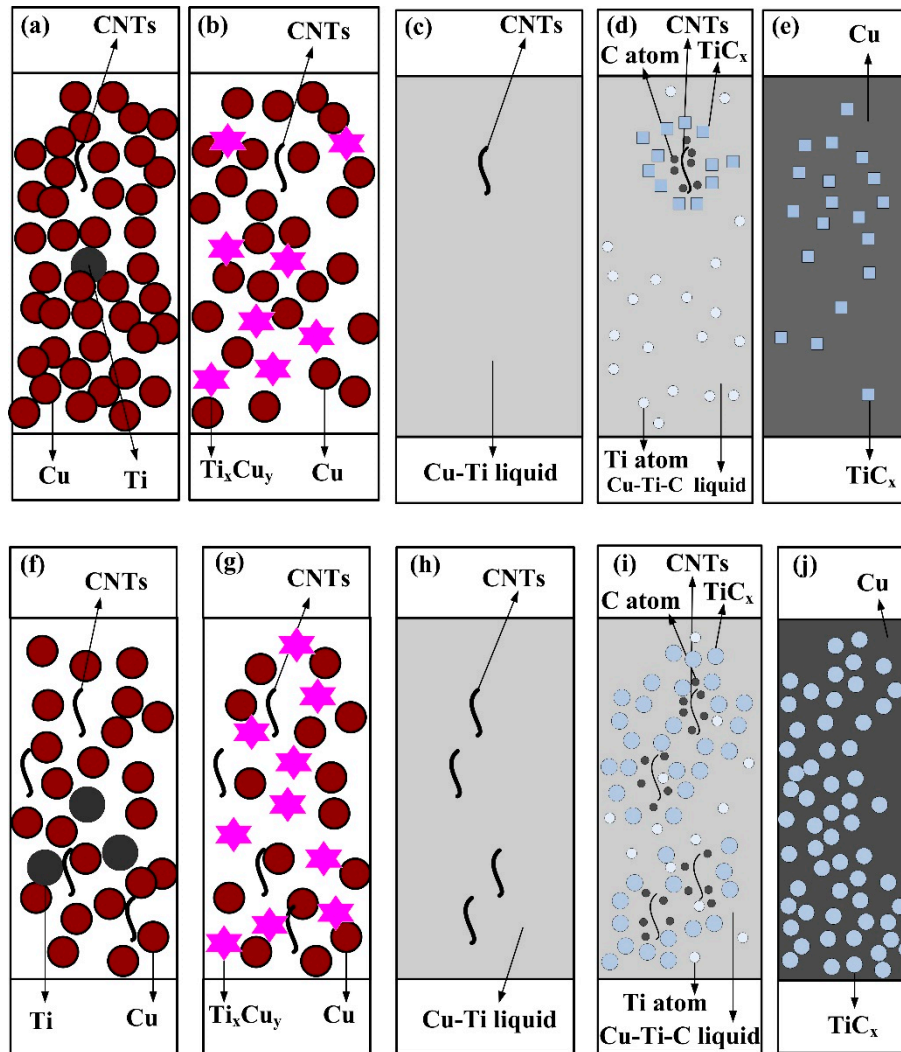


Figure 8. Models of the reaction mechanism with different Cu contents: (a–e) high Cu content, (f–j) low Cu content, (a,f) initial reactants, (b,g) the formation of Ti_xCu_y compounds (c,h) the formation of Cu-Ti liquid, (d,i) TiC_x particulates gradually precipitated out of the liquid and (e,j) fully reacted.

A sketch map for the morphology evolution mechanism of in situ TiC_x particles was introduced according to the previous study, as shown in Figure 9. The morphology of in situ TiC_x changed in the order of octahedron, close-to-sphere, sphere and cube with the increasing of the C/Ti molar ratio and in the order of close-to-spherical, spherical and cubic with the increasing of Cu content. The two-dimensional (2D) nucleation growth was the main growth means of TiC_x particles due to the high combustion temperature in the Cu-Ti-C system. The {111} surface in TiC_x is an alternate arrangement of the Ti atomic layer and the C atomic layer. Since the Ti-terminated surface is more stable than the C-terminated surface, the outmost terminated surface of the TiC_x {111} surface is usually a Ti atomic layer [43,44]. Thus, when two-dimensional crystal nuclei are formed on the {111} surface of TiC_x , the formation of C atomic layers is more difficult than that of Ti atomic layers. Thus, the key step in two-dimensional crystal nucleation is the formation of the C atomic layer. Moreover,

the decisive factor for the formation of the C atomic layer and for two-dimensional crystal nucleation is the concentration of C ($[C]$) in the Cu-Ti-C liquid phase. During the formation and growth of TiC_x nuclei, when $[C]$ is low, the TiC_x particles tend to grow into the two-dimensional nuclei on the $\{100\}$ surface, so the $\{100\}$ plane gradually shrinks and stabilizes, finally forming octahedrons surrounded by $\{111\}$ surfaces. With the increase of $[C]$, the TiC_x particles tend to grow into the two-dimensional nuclei on the $\{111\}$ plane. As a result, the $\{111\}$ surface gradually shrinks and stabilizes, but its distance from the center is gradually enlarged. Thus, the $\{111\}$ surface atop TiC_x particles is gradually shrinking and exposed, finally forming a cube surrounded by $\{100\}$ surfaces. As a result, the morphologies of in situ TiC_x particles changed in the order of octahedron, close-to-sphere, sphere and cube with the increasing of the C/Ti atom ratio in the Cu-Ti-C ternary liquid.

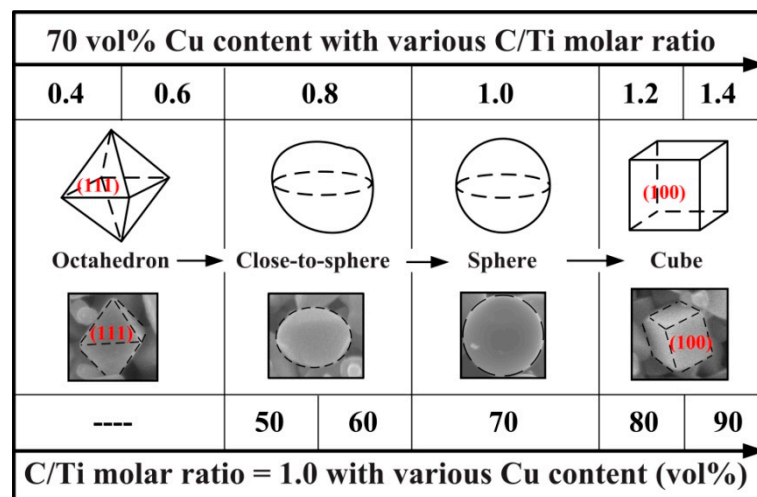


Figure 9. Sketch map of the morphology evolution mechanism of the in situ TiC_x particles in the Cu-Ti-C system.

4. Conclusions

TiC_x/Cu composites with various particle morphologies were successfully fabricated by combining TE and HP methods in the Cu-Ti-C system. Octahedral, spherical or cube-shaped TiC_x particles were synthesized by altering the Cu content and C/Ti molar ratio. The shape of TiC_x particles is octahedral at C/Ti molar ratios from 0.4–0.6 with the presence of 70 vol% Cu, spherical and close-to-spherical at C/Ti molar ratios from 0.8–1.0 with the presence of 70 vol% Cu and cubic at C/Ti molar ratios ≥ 1.0 with the presence of Cu from 70 vol%–90 vol%. The shape of TiC_x particles was theoretically determined by the x value of TiC_x . The x value was affected by the C/Ti molar ratio of the reactant to a certain extent. A carbon-rich or carbon-depleted environment was created by changing the C/Ti molar ratio and Cu content of the reactant so as to control the shape of in situ TiC_x particles. A carbon-rich environment provided the conditions to form cube-shaped TiC_x during the in situ reaction process. On the other hand, the carbon-depleted environment provided the conditions to form octahedrally-shaped TiC_x during the in situ reaction process. The morphologies of in situ TiC_x particles changed in the order of octahedral, close-to-spherical, spherical and cubic with the increasing of the C/Ti atom ratio in the Cu-Ti-C ternary liquid, which was influenced by the C/Ti molar ratio in the reactant. When the C/Ti molar ratio is constant, the shape of the TiC_x particles gradually changes from cube, close-to-sphere, to sphere with the decrease of Cu content. The slow reaction speed of the high Cu content provided a carbon-rich environment in the Cu-Ti-C ternary liquid and formed cube-shaped TiC_x . The fast reaction speed of low Cu content dissolves less $[C]$ atoms than the high Cu content, did not leave enough time for the carbon source to dissolve into the Cu-Ti-C ternary liquid and provided an environment with fewer carbon atoms compared with the carbon-rich environment, finally forming close-to-spherical TiC_x .

Acknowledgments: This work is supported by the National Natural Science Foundation of China (NNSFC, No. 51571101). Partial financial supports come from the “twelfth five-year plan” Science & Technology Research Foundation of Education Bureau of Jilin Province, China (Grant No. 2015-478) and the Project 985-High Properties Materials of Jilin University.

Author Contributions: Dongdong Zhang and Jinguo Wang conceived and designed the experiments. Dongdong Zhang, Haolong Liu, Fang Bai and Yong Wang performed the experiments. Dongdong Zhang, Liping Sun and Jinguo Wang analyzed the data. Dongdong Zhang wrote the paper. Liping Sun polished the manuscript.

Conflicts of Interest: The authors declare no conflict of interest.

References

1. Rahaei, M.B.; Yazdanirad, R.; Kazemzadeh, A.; Ebadzadeh, T. Mechanochemical synthesis of nano TiC powder by mechanical milling of titanium and graphite powders. *Powder Technol.* **2012**, *217*, 369–376. [[CrossRef](#)]
2. Yang, Y.F.; Mu, D.K.; Jiang, Q.C. A simple route to fabricate TiC-TiB₂/Ni composite via thermal explosion reaction assisted with external pressure in air. *Mater. Chem. Phys.* **2014**, *143*, 480–485. [[CrossRef](#)]
3. Klinger, L.; Gotman, I.; Horvitz, D. In-situ processing of TiB₂: TiC ceramic composites by thermal explosion under pressure: experimental study and modeling. *Mater. Sci. Eng. A* **2001**, *302*, 92–99. [[CrossRef](#)]
4. Lin, Q.L.; Shen, P.; Yang, L.L.; Jin, S.B.; Jiang, Q.C. Wetting of TiC by molten Al at 1123–1323 K. *Acta Mater.* **2011**, *59*, 1898–1911. [[CrossRef](#)]
5. Yang, Y.F.; Jiang, Q.C. Reaction behaviour, microstructure and mechanical properties of TiC-TiB₂/Ni composite fabricated by pressure assisted self-propagating high-temperature synthesis in air and vacuum. *Mater. Des.* **2013**, *49*, 123–129. [[CrossRef](#)]
6. Shu, S.L.; Yang, H.Y.; Tong, C.Z.; Qiu, F. Fabrication of TiC_x-TiB₂/Al Composites for Application as a Heat Sink. *Materials* **2016**, *9*, 642. [[CrossRef](#)]
7. Goh, C.S.; Chong, W.L.E.; Lee, T.K.; Breach, C. Corrosion Study and Intermetallics Formation in Gold and Copper Wire Bonding in Microelectronics Packaging. *Crystals* **2013**, *3*, 391–404. [[CrossRef](#)]
8. Wang, L.; Qiu, F.; Zhao, Q.L.; Wang, H.Y.; Yang, D.L.; Jiang, Q.C. Simultaneously increasing the elevated-temperature tensile strength and plasticity of in situ nano-sized TiC_x/Al-Cu-Mg composites. *Mater. Charact.* **2017**, *125*, 7–12. [[CrossRef](#)]
9. Kampe, S.L.; Christodoulou, J.; Feng, C.R.; Christodoulou, L.; Michel, D.J. The effect of matrix microstructure and reinforcement shape on the creep deformation of near- γ titanium aluminide composites. *Acta Mater.* **1998**, *46*, 2881–2894. [[CrossRef](#)]
10. Chen, C.R.; Qin, S.Y.; Li, S.X.; Wen, J.L. Finite element analysis about effects of particle morphology on mechanical response of composites. *Mater. Sci. Eng. A* **2000**, *278*, 96–105. [[CrossRef](#)]
11. Tirtom, I.; Guden, M.; Yildiz, H. Simulation of the strain rate sensitive flow behavior of SiC-particulate reinforced aluminum metal matrix composites. *Comp. Mater. Sci.* **2008**, *48*, 570–578. [[CrossRef](#)]
12. Meijer, G.; Ellyin, F.; Xia, Z. Aspects of residual thermal stress/strain in particle reinforced metal matrix composites. *Compos. Part B-Eng.* **2000**, *31*, 29–37. [[CrossRef](#)]
13. Qiu, F.; Han, Y.; Cheng, A.; Lu, J.B.; Jiang, Q.C. Effect of Cr Content on the Compression Properties and Abrasive Wear Behavior of the High-Volume Fraction (TiC-TiB₂)/Cu Composites. *Acta Metall. Sin.* **2014**, *27*, 951–956. [[CrossRef](#)]
14. Zhao, Q.; Liang, Y.H.; Zhang, Z.H.; Li, X.J.; Ren, L.Q. Effect of Al content on impact resistance behavior of Al-Ti-B₄C composite fabricated under air atmosphere. *Micron* **2016**, *91*, 11–21. [[CrossRef](#)] [[PubMed](#)]
15. Wang, L.; Qiu, F.; Ouyang, L.C.; Wang, H.Y.; Zha, M.; Shu, S.L.; Zhao, Q.L.; Jiang, Q.C. A Novel Approach of Using Ground CNTs as the Carbon Source to Fabricate Uniformly Distributed Nano-Sized TiC_x/2009Al Composites. *Materials* **2015**, *8*, 8839–8849. [[CrossRef](#)]
16. Liang, Y.H.; Zhao, Q.; Zhang, Z.H.; Han, Z.W.; Li, X.J.; Ren, L.Q. In-situ fabrication of TiC-TiB₂ precipitates in Mn-steel using thermal explosion (TE) casting. *J Mater. Res.* **2015**, *30*, 1019–1028. [[CrossRef](#)]
17. Liang, Y.H.; Zhao, Q.; Li, X.J.; Zhang, Z.H.; Ren, L.Q. Effect of Ti and C particle size on reaction behavior of thermal explosion (TE) reaction of Cu-Ti-C system under Ar and air atmosphere. *J Alloy Compd.* **2016**, *679*, 65–73. [[CrossRef](#)]

18. Yang, Y.F.; Wang, H.Y.; Wang, J.G.; Jiang, Q.C. Effect of C particle size on the mechanism of self-propagation high-temperature synthesis in the Ni–Ti–C system. *J Alloy Compd.* **2011**, *509*, 7060–7065. [[CrossRef](#)]
19. Wang, L.; Qiu, F.; Liu, J.Y.; Wang, H.Y.; Wang, J.G.; Zhu, L.; Jiang, Q.C. Microstructure and tensile properties of in situ synthesized nano-sized TiC_x/2009Al composites. *Mater. Des.* **2015**, *79*, 68–72. [[CrossRef](#)]
20. Shu, S.L.; Tong, C.Z.; Qiu, F.; Jiang, Q.C. Effect of Ceramic Content on the Compression Properties of TiB₂-Ti₂AlC/TiAl Composites. *Metals* **2015**, *5*, 2200–2209. [[CrossRef](#)]
21. Jin, S.B.; Shen, P.; Zou, B.L.; Jiang, Q.C. Morphology Evolution of TiC_x Grains During SHS in an Al-Ti-C System. *Cryst. Growth Des.* **2009**, *9*, 646–649. [[CrossRef](#)]
22. Nie, J.F.; Wu, Y.Y.; Li, P.T.; Li, H.; Liu, X.F. Morphological evolution of TiC from octahedron to cube induced by elemental nickel. *CrystEngComm* **2012**, *14*, 2213–2221. [[CrossRef](#)]
23. Wang, L.; Qiu, F.; Shu, S.L.; Zhao, Q.L.; Jiang, Q.C. Effects of different carbon sources on the compressive properties of in situ high-volume-fraction TiC_x /2009Al composites. *Powder Metall.* **2016**, *59*, 370–375. [[CrossRef](#)]
24. Zhao, Q.; Liang, Y.H.; Zhang, Z.H.; Li, X.J.; Ren, L.Q. Study on the Impact Resistance of Bionic Layered Composite of TiC-TiB₂/Al from Al-Ti-B₄C System. *Materials* **2016**, *9*, 708. [[CrossRef](#)]
25. Zhao, Q.; Liang, Y.H.; Zhang, Z.H.; Li, X.J.; Ren, L.Q. Microstructure and Dry-Sliding Wear Behavior of B₄C Ceramic Particulate Reinforced Al 5083 Matrix Composite. *Metals* **2016**, *6*, 227. [[CrossRef](#)]
26. Zhou, D.S.; Qiu, F.; Jiang, Q.C. Simultaneously increasing the strength and ductility of nano-sized TiN particle reinforced Al–Cu matrix composites. *Mater. Sci. Eng. A* **2014**, *596*, 98–102. [[CrossRef](#)]
27. Qiu, F.; Chu, J.G.; Hu, W.; Lu, J.B.; Li, X.D.; Han, Y.; Jiang, Q.C. Study of effect of Zr addition on the microstructures and mechanical properties of (TiC_x-TiB₂)/Cu composites by combustion synthesis and hot press consolidation in the Cu–Ti–B₄C–Zr system. *Mater. Res. Bull.* **2015**, *70*, 167–172. [[CrossRef](#)]
28. Shojaeepour, F.; Abachi, P.; Purazrang, K.; Moghanian, A.H. Production and properties of Cu/Cr₂O₃ nano-composites. *Powder Technol.* **2012**, *222*, 80–84. [[CrossRef](#)]
29. Besterici, M.; Ivan, J.; Kovac, L.; Weissgaerber, T.; Sauer, C. Strain and fracture mechanism of Cu–TiC. *Mater. Lett.* **1999**, *38*, 270–274. [[CrossRef](#)]
30. Akhtar, F.; Askari, S.J.; Shah, K.A.; Du, X.L.; Guo, S.J. Microstructure, mechanical properties, electrical conductivity and wear behavior of high volume TiC reinforced Cu-matrix composites. *Mater. Charact.* **2009**, *60*, 327–366. [[CrossRef](#)]
31. Liu, Q.; He, X.B.; Ren, S.B.; Liu, T.T.; Kang, Q.P.; Qu, X.H. Fabrication and thermal conductivity of copper matrix composites reinforced with Mo₂C or TiC coated graphite fiber. *Mater. Res. Bull.* **2013**, *48*, 4811–4817. [[CrossRef](#)]
32. Wang, L.; Qiu, F.; Zhao, Q.L.; Zha, M.; Jiang, Q.C. Superior high creep resistance of in situ nano-sized TiC_x/Al-Cu-Mg composite. *Sci. Rep.* **2017**, *7*, 4540. [[CrossRef](#)] [[PubMed](#)]
33. Zhou, D.S.; Jin, S.B.; Li, Y.J.; Qiu, F.; Deng, F.; Wang, J.G.; Jiang, Q.C. Effect of stoichiometry on the surface energies of {100} and {111} and the crystal shape of TiC_x and TiN_x. *CrystEngComm* **2013**, *15*, 643–649. [[CrossRef](#)]
34. Arya, A.; Carter, E.A. Structure, bonding, and adhesion at the TiC (100)/Fe (110) interface from first principles. *J Chem. Phys.* **2003**, *118*, 8982–8996. [[CrossRef](#)]
35. Zhang, D.D.; Bai, F.; Sun, L.P.; Wang, Y.; Wang, J.G. Compression properties and electrical conductivity of in-situ 20 vol% nano-sized TiC_x/Cu composites with different particle size and morphology. *Materials* **2017**, *10*, 499. [[CrossRef](#)]
36. Qiu, F.; Gao, Y.Y.; Liu, J.Y.; Shu, S.L.; Zou, Q.; Zhang, T.Z.; Jiang, Q.C. Effect of C/Ti ratio on the compressive properties and wear properties of the 50 vol. % submicron-sized TiC_x/2014Al composites fabricated by combustion synthesis and hot press consolidation. *Powder Metall.* **2016**, *59*, 256–261. [[CrossRef](#)]
37. Degtyareva, V.F.; Afonikova, N.S. Simple Metal and Binary Alloy Phases Based on the fcc Structure: Electronic Origin of Distortions, Superlattices and Vacancies. *Crystals* **2017**, *7*, 34. [[CrossRef](#)]
38. Liu, L.M.; Wang, S.Q.; Ye, H.Q. First-principles study of polar Al/TiN (111) interfaces. *Acta Mater.* **2004**, *52*, 3618–3688. [[CrossRef](#)]
39. Merzhanov, A.G. The chemistry of self-propagating high-temperature synthesis. *J. Mater. Chem.* **2004**, *14*, 1779–1786. [[CrossRef](#)]
40. Liang, Y.H.; Han, Z.W.; Zhang, Z.H.; Li, X.J.; Ren, L.Q. Study on the reaction mechanism of self-propagating high-temperature synthesis of TiC in the Cu-Ti-C system. *Mater. Chem. Phys.* **2012**, *137*, 200–206. [[CrossRef](#)]

41. Liang, Y.H.; Zhao, Q.; Zhang, Z.H.; Li, X.J.; Ren, L.Q. Effect of B₄C particle size on the reaction behavior of self-propagation high-temperature synthesis of TiC-TiB₂ ceramic/Cu composites from a Cu-Ti-B₄C system. *Int. J. Refract. Met. H.* **2014**, *46*, 71–79. [[CrossRef](#)]
42. Yang, Y.F.; Jiang, Q.C. Effect of TiB₂/TiC ratio on the microstructure and mechanical properties of high volume fractions of TiB₂/TiC reinforced Fe matrix composite. *Int. J. Refract. Met. H.* **2013**, *38*, 137–139. [[CrossRef](#)]
43. Johansson, L.I. Electronic and structural properties of transition-metal carbide and nitride surfaces. *Surf. Sci. Rep.* **1995**, *21*, 177–250. [[CrossRef](#)]
44. Tan, K.E.; Finnis, M.W.; Horsfield, A.P.; Sutton, A.P. Why TiC (111) is observed to be Ti terminated. *Surf. Sci.* **1996**, *348*, 49–54. [[CrossRef](#)]



© 2017 by the authors. Licensee MDPI, Basel, Switzerland. This article is an open access article distributed under the terms and conditions of the Creative Commons Attribution (CC BY) license (<http://creativecommons.org/licenses/by/4.0/>).